Biophysical *Journal*
Article

Biophysical Society

Cosolute modulation of protein oligomerization reactions in the homeostatic timescale

Borja Mateos,[1,2] Ganeko Bernardo-Seisdedos,[1] Valentin Dietrich,[3] Nicanor Zalba,[1] Gabriel Ortega,[4] Francesca Peccati,[5] Gonzalo Jiménez-Osés,[5] Robert Konrat,[2] Martin Tollinger,[3] and Oscar Millet[1,*]

[1]Precision Medicine and Metabolism Laboratory, CIC bioGUNE, Basque Research and Technology Alliance, Parque Tecnológico de Bizkaia, Derio, Spain; [2]Department of Structural and Computational Biology, University of Vienna, Max Perutz Labs, Vienna Biocenter Campus 5, Vienna, Austria; [3]Center of Molecular Biosciences and Institute of Organic Chemistry, University of Innsbruck, Innsbruck, Austria; [4]Department of Chemistry and Biochemistry, University of California, Santa Barbara, California; and [5]Computational Chemistry Laboratory, CIC bioGUNE, Basque Research and Technology Alliance, Parque Tecnológico de Bizkaia, Derio, Spain

ABSTRACT Protein oligomerization processes are widespread and of crucial importance to understand degenerative diseases and healthy regulatory pathways. One particular case is the homo-oligomerization of folded domains involving domain swapping, often found as a part of the protein homeostasis in the crowded cytosol, composed of a complex mixture of cosolutes. Here, we have investigated the effect of a plethora of cosolutes of very diverse nature on the kinetics of a protein dimerization by domain swapping. In the absence of cosolutes, our system exhibits slow interconversion rates, with the reaction reaching the equilibrium within the average protein homeostasis timescale (24–48 h). In the presence of crowders, though, the oligomerization reaction in the same time frame will, depending on the protein's initial oligomeric state, either reach a pure equilibrium state or get kinetically trapped into an apparent equilibrium. Specifically, when the reaction is initiated from a large excess of dimer, it becomes unsensitive to the effect of cosolutes and reaches the same equilibrium populations as in the absence of cosolute. Conversely, when the reaction starts from a large excess of monomer, the reaction during the homeostatic timescale occurs under kinetic control, and it is exquisitely sensitive to the presence and nature of the cosolute. In this scenario (the most habitual case in intracellular oligomerization processes), the effect of cosolutes on the intermediate conformation and diffusion-mediated encounters will dictate how the cellular milieu affects the domain-swapping reaction.

SIGNIFICANCE Under stress conditions, proteins tend to misfold and aggregate as a consequence of their inherent stability and their interaction with the crowded cytosol. Domain swapping implies protein unfolding coupled with oligomerization, and it constitutes a paradigm for the different mechanisms that a protein will undergo during its homeostasis. We have investigated the effect of a large set of cosolutes of diverse nature in the domain-swapping reaction of a model protein. The crowder effect on the kinetics of the protein homo-oligomerization reaction depends on the initial protein oligomeric state. These results provide insight to understand the regulation of the homo-oligomerization reactions in complex solvent mixtures, such as the crowded cytosol, where protein gradients often occur as a function of space and time.

INTRODUCTION

Proteins and nucleic acids thrive and exert their function in the crowded environment of living cells (1). Such solvents, typically the cytosol, are generically composed of a sum of cosolutes that comprise all kinds of biological macromolecules, metabolites, and salts, among other species. Moreover, the cytosol is a noninert environment with dynamic composition turnovers. Under stress conditions, many cells are able to accumulate protective or stabilizing osmolytes (2), whereas a given transient adverse cellular composition may also trigger the formation of toxic species (i.e., amyloids) (3–6). Thus, the stability and the functional activity of a protein in the cellular milieu (i.e., its homeostasis) arise from a delicate balance between the intrinsic properties of the polypeptide chain and its interaction with the crowded cytosol.

A highly developed theoretical framework has been developed to explain the effect of cosolutes in biomolecular stability (7–10) and kinetic rates (11,12). The multiple

Submitted January 19, 2021, and accepted for publication March 25, 2021.

*Correspondence: omillet@cicbiogune.es

Borja Mateos, Ganeko Bernardo-Seisdedos, and Valentin Dietrich contributed equally to this work.

Editor: Robert Best.

https://doi.org/10.1016/j.bpj.2021.03.020

mechanisms that simultaneously contribute to the nonideal behavior induced by the crowding agents is a reflection of the inherent complexity of the biological systems. For example, recent in-cell experimental evidence has reported a priori unexpected effects on the catalytic activity (13) and oligomerization (14).

From a thermodynamic point of view, the chemical potential (ΔG) deviates from the standard state reference value (ΔG^0) according to the expression

$$\begin{aligned}\Delta G &= \Delta G^0 + \Delta G^{ideal} + \Delta G^{nonideal} \\ &= \Delta G^0 + RTln(C) + RTln(\gamma).\end{aligned} \quad (1)$$

The nonideal character of the solution is expressed by the activity coefficient (γ), defined as the ratio between the thermodynamic concentration (activity, a) and the actual concentration in the mixture (C). These effects tend to be nonlinear with respect to the cosolute concentration, affecting more biomolecules rather than small molecules. Two main mechanisms may alter the thermodynamic equilibrium and contribute to the deviation of the activity coefficient from unity (which represents the ideal case). Macromolecular crowding often refers to the excluded volume effects generated by steric repulsion, and it plays a pivotal role in the homeostasis of the biomolecules (8,15,16). In turn, an increasing number of studies underline the nonvanishing role of the weak nonspecific interactions between cosolutes and protein probes (9,17–19). Both mechanisms may alter the thermodynamic equilibrium, and theoretical statistical-thermodynamic models are used to predict the activity coefficients (20,21). Those models are ultimately expressed in terms of the excluded volume differences (ΔV) of the equilibrium conformations (7,20) and the differences of accessible surface area (ΔASA) (18). Theoretically and empirically (12,22), a crowded medium may also slow down the rotational and translational diffusion motions of the biomolecule. In multimolecular reactions requiring particle collision, diffusion will decrease the rate of formation of the encounter complex in a manner dependent on the concentration of the crowding agent (22). Yet, this effect occurs primarily by changes in the hydrodynamic properties of the solution and not through an effect on the activity coefficients (23,24).

Domain swapping, understood as a paradigm of protein oligomerization, requires two or more protein molecules to form a dimer or higher oligomer by exchanging an identical structural element, also called domains. Importantly, domain-swapping mechanisms are functionally relevant because they imply intermediate conformations with partial or total unfolding (25,26) and have been in involved in important biological processes such as amyloid fibril formation (27) and fold-switching oligomerization (28). Despite the domain-swapped thermodynamic stability having been rationalized in terms of protein shape (29,30) or crowding interactions (31), most of the natural domain-swapped oligomers display extremely slow off rates, thus hardly achieving the equilibrium populations in a biological timescale (homeostasis).

Here, we have investigated the interplay between cosolutes and the protein oligomerization kinetics. Specifically, we have experimentally tested the effect of a plethora of cosolutes including denaturants, Hofmeister ions, and osmolytes (also here identified as crowders; Table S1) in the kinetics of the fold-swapping equilibrium, produced by a mutant of the immunoglobulin G binding B1 domain of protein L from *Streptococcus magnus* (32,33) ($ProtL_{G55A}$). Previously, it was described that the domain swapping of $ProtL_{G55A}$ requires a certain degree of decompaction to accomplish the transition between two monomer units, in agreement with the common notion that (local) unfolding is a prerequisite for domain swapping (25,32). Here, we focus on the implications of such mechanism in the stability of oligomers. This system offers the advantage that high-resolution structures are available for the two species (Protein Data Bank, PDB: 1HZ5 (monomer) and 1K51 (dimer)). The excluded volume and accessible area differences between the monomer and the dimer are negligible for the range of small cosolutes tested (Table S3) and irrelevant for the model (Fig. 1 *A*; Eq. 8). Conversely, more applicable should be the differences in volume and area with respect low-populated and partially unfolded intermediate state(s). However, the structural characterization of those states is hardly achievable. Although NMR spectroscopy is a well-suited tool to identify low-populated (excited) states in proteins (34), the identification of intermediates was not achieved so far. For example, backbone amide ^{15}N relaxation dispersion measurements of $ProtL_{G55A}$ yield flat dispersion profiles for all backbone amide resonances, indicating that both forms of the protein are conformationally homogeneous on the micro-to-millisecond timescale (32).

As a key innovation in our experimental design, we have interrogated the effect of cosolutes on the homo-oligomerization reaction by starting from two opposite initial conditions. We have monitored by real-time NMR spectroscopy the monomer-dimer interconversion during a realistic biological timescale (i.e., protein half-lives range an average of 0.5–35 h in dividing mammalian cells (35)). Our results show that the kinetic rates of dimer and monomer depend not only on the nature and concentration of the cosolute but mainly on the initial reaction conditions, hereafter referred to as the initial protein oligomeric state, obtaining very different cosolute effects depending on whether we start from the dimeric or the monomeric species. This apparently counterintuitive result can be rationalized in terms of the reaction mechanism and the existence of a largely unfolded intermediate. The apparent equilibrium reached in the biological timescale underlines the importance of stoichiometry in the effect of crowders (and eventually the cytosol) on the kinetics and stability of chemical reactions, including oligomerization processes that intervene in, for example, amyloid formation.

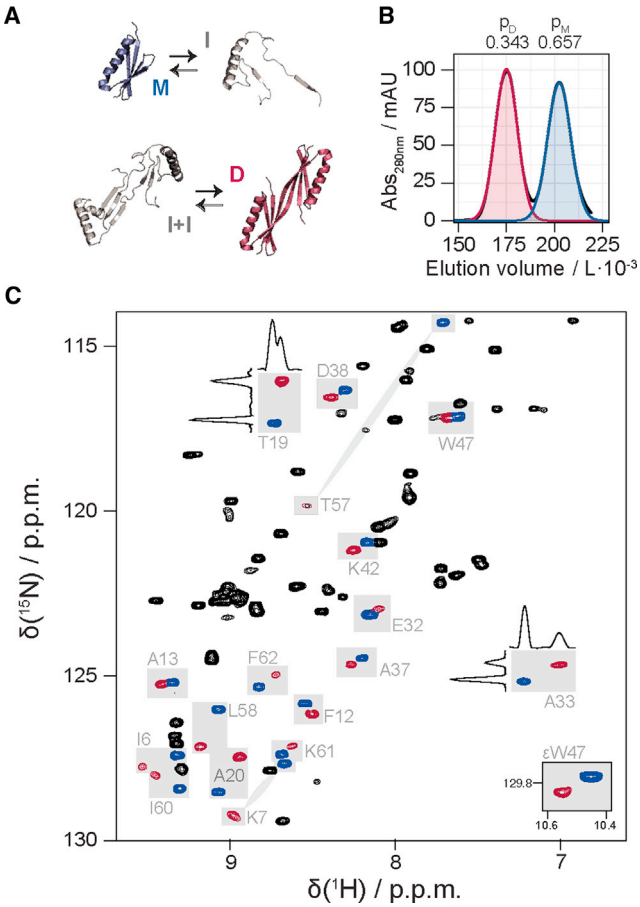

FIGURE 1 Domain swapping of protein L mutant G55A (ProtL$_{G55A}$). (*A*) Schematic representation of the oligomerization reaction starting from monomer (*blue*) and dimer (*red*) and also representing the intermediate (*gray*). (*B*) SEC profile of a sample equilibrated at room temperature (>48 h). Approximately one-third of protein molecules dimerize and can be purified independently because of the chromatographic separation. Populations are obtained from a Gaussian fit to the peaks. (*C*) Region of ^{1}H-^{15}N HSQC spectra recorded on ^{15}N-labeled ProtL$_{G55A}$ at equilibrium. Unambiguous assignment of isolated peaks is indicated in blue for monomer and red for dimer. Representative ^{1}H-^{15}N HSQC spectra of pure monomer and dimer are plotted in Fig. S1.

MATERIALS AND METHODS

Sample preparation

ProtL$_{G55A}$ was prepared as previously described (32). Monomer and dimer populations were separated by size-exclusion chromatography (HiLoad 26/600 Superdex 75 pg (GE Healthcare, Chicago, IL)). The final samples were buffer exchanged to 20 mM phosphate buffer at pH 6.0 and aliquoted in samples of 500 μL at 500 μM. The aliquots were immediately lyophilized and stored at −20°C. NMR samples were prepared by hydrating the lyophilized powder in a water solution with or without the desired cosolute and 7% D_2O.

NMR spectroscopy

NMR data were collected at on an 800-MHz Bruker Avance III spectrometer (Bruker, Rheinstetten, Germany) equipped with a cryoprobe and on a 600-MHz Bruker Avance III US2 spectrometer. Acquisition parameters are provided in Table S4. Processing was carried out with NMRPipe (36). Processing parameters are provided in Table S5. Spectral analysis of the data was performed with CcpNmr (37). Several residue H^N signals have been selected based on their well-separated signals as reporters of monomer and dimer forms (E2, I6, K7, F12, A13, T19, A20, G24, A33, A37, D38, K42, Y47, L58, I60, K61, and F62). The complete table of experimental conditions is appended in Table S6. Statistical analysis was conducted using MATLAB (The MathWorks, Natick, MA) and R.

Cosolute hydrodynamic radius calculation

The R_h for each tested cosolute was extracted from diffusion NMR experiments to measure translational diffusion (D_T). A DOSY spectrum was recorded with 5 mM of cosolute in 20 mM phosphate buffer at pH 6 with 1 μM of sodium azide and 40 μM of DSS-d_6 (internal reference). The estimated viscosity ratio of H_2O/D_2O 0.93:0.07 at 25°C was calculated as proposed by Hardy and Cottington (38). A DSS-d_6 singlet at 0 ppm was used as internal reference standard in the diffusion dimension ($D_T = -9.1412$ log(m^2/s)). DSS has the advantage of keeping a relatively constant D_T over a wide range of deuterium content and pH (39). R_h was calculated by solving the Stokes-Einstein equation:

$$R_h = \frac{k_B T}{6\pi\eta D_T}, \tag{2}$$

where k_B is the Boltzmann constant (1.3806×10^{-23}(m^2 • kg/s^2 • K). Fig. S5 and Table S3 contain the measured diffusion for each cosolute (when more than one signal was observed, the average was calculated). For ions, the thermochemical radii were extracted from previously reported values (40,41) (K^+ = 1.33 Å, Na^+ = 1.02 Å, Cl^- = 1.81 Å, SO_4^{2-} = 2.18 Å, and SCN^- = 2.09 Å). The R_h of water, assuming no water shell around the molecule (slip boundary condition), is reported to be 1.64 Å at 25°C (42). For the stick condition, the $H_2{}^{17}O$ radius has been reported to be 1.21 Å; in any case, it does not drastically change the calculations reported. The excluded volume differences for the cosolutes tested on the ProtL$_{G55A}$ system (Table S3) were calculated using the ProteinVolume tool (43). The ASA differences were calculated using Pymol.

Accelerated molecular dynamics simulations

The x-ray diffraction structures of the B1 domain of protein L from *Peptostreptococcus magnus* (PDB: 1HZ5) and a variant in which the G55A mutation induces B1 domain swapping (PDB: 1K51; Ala55 reverted to the native Gly in the simulations) were used as initial geometries. Molecular dynamics simulations were run with the AMBER suite (44), using the *ff14SB* (45) force field. Initial structures were neutralized with either Na^+ or Cl^- ions and set at the center of a cubic TIP3P water (46) box with a buffering distance between solute and box of 10 Å. For each complex, a two-stage geometry optimization approach was followed: the first stage minimizes only the positions of solvent molecules and ions, and the second stage is an unrestrained minimization of all the atoms in the simulation cell. The systems were then heated by incrementing the temperature from 0 to 300 K along 1 ns under a constant pressure of 1 atm and periodic boundary conditions. Harmonic restraints of 10 kcal mol^{-1} were applied to the solute under the Andersen temperature coupling scheme (47,48). Water molecules were treated with the SHAKE algorithm (49) such that the angle between the hydrogen atoms is kept fixed through the simulations. Long-range electrostatic effects were modeled using the particle mesh Ewald method (50). An 8 Å cutoff was applied to the Lennard-Jones interactions. Each system was equilibrated for 2 ns with a 2 fs time step at a constant volume and temperature of 300 K. After equilibration using conventional molecular dynamics (cMD), a Gaussian accelerated molecular dynamics (GaMD) protocol (51,52) designed to enhance conformational sampling by adding a harmonic boost potential to smooth the system potential energy surface,

was applied. This protocol consisted of an initial cMD pre-equilibration stage of 2 ns, in which the boost potential is applied and the boost parameters are not updated, and a second pre-equilibration stage of 50 ns, in which the boost potential is applied and boost parameters are updated (*igamd* = 3, *iE* = 1, *irest_gamd* = 0, *sigma0P* = 6.0, *sigma0D* = 6.0, *ntave* = 200,000, *ntcmdprep* = 200,000, *ntcmd* = 1,000,000, *ntebprep* = 800,000, *nteb* = 25,000,000). In the final production stage (90–100 μs), the boost potential is applied and the boost parameters obtained from the GaMD equilibration are not updated (*igamd* = 3, *iE* = 1, *irest_gamd* = 1, *sigma0P* = 6.0, *sigma0D* = 6.0, *ntave* = 200,000, *ntcmdprep* = 0, *ntcmd* = 0, *ntebprep* = 0, *nteb* = 0). The GaMD trajectories were run in the NVT ensemble at 300 K with a time step of 2 fs using the Andersen thermostat. The applied potential was a dual boost on both dihedral and total potential energy. Representative geometries, molecular surfaces, and volumes were extracted from the trajectories using the *cpptraj* module of AMBER.

Steady-state kinetic equations

The derivatization for homodimerization kinetic equations were carried out in previous work (32). The corresponding time-course monomeric and dimeric populations for the association pseudoequilibrium are

$$c_M(t) = c_0 - 2\frac{\lambda_1\lambda_2(1 - e^{-(4k_{asc}(\lambda_1-\lambda_2)t)})}{\lambda_1 - \lambda_2 e^{-(4k_{asc}(\lambda_1-\lambda_2)t)}} \quad (3)$$

and

$$c_D(t) = \frac{\lambda_1\lambda_2(1 - e^{-(4k_{asc}(\lambda_1-\lambda_2)t)})}{\lambda_1 - \lambda_2 e^{-(4k_{asc}(\lambda_1-\lambda_2)t)}} \quad (4)$$

and for the dissociation pseudoequilibrium are

$$c_M(t) = c_0 - 2\frac{\lambda_2(1-\lambda_1) + \lambda_1(\lambda_2 - 1)e^{-(4k_{asc}(\lambda_1-\lambda_2)t)}}{(1-\lambda_1) + (\lambda_2 - 1)e^{-(4k_{asc}(\lambda_1-\lambda_2)t)}} \quad (5)$$

and

$$c_D(t) = \frac{\lambda_2(1-\lambda_1) + \lambda_1(\lambda_2 - 1)e^{-(4k_{asc}(\lambda_1-\lambda_2)t)}}{(1-\lambda_1) + (\lambda_2 - 1)e^{-(4k_{asc}(\lambda_1-\lambda_2)t)}}, \quad (6)$$

with

$$\lambda_{1/2} = \frac{1}{2}\left(\frac{k_{diss}}{4k_{asc}} + c_0\right) \pm \sqrt{\frac{1}{4}\left(\frac{k_{diss}}{4k_{asc}} + c_0\right)^2 - \frac{1}{4}(c_0)^2}, \quad (7)$$

where $c_M(t)$ and $c_D(t)$ were normalized so $c_M(t)+2c_D(t) = c_0 = 1$. Kinetic rates (k_{asc} and k_{diss}) were extracted from fitting Eq. 3–6 to real-time NMR peak volumes of the corresponding association or dissociation reactions. Although the monomer and dimer protein samples were highly pure and homogeneous, the first data points of the time series were normalized by the extrapolated value at t = 0 to ensure the correct fitting.

RESULTS

ProtL$_{G55A}$ domain swapping under reference conditions

ProtL$_{G55A}$ exists in equilibrium between its monomeric and domain-swapped dimeric form (Fig. 1 *A*). The interconversion is slow enough (with a half-time for the interconversion of ~2 h in the reference buffer) to allow the separation and purification of monomer and dimer by size-exclusion chromatography (SEC) (Fig. 1 *B*). Gaussian fit and integration of the protein's SEC profile at equilibrium showed a monomer (p_M) and a dimer (p_D) population of 0.657 and 0.343, respectively.

We also investigated the reaction kinetics using NMR spectroscopy. To monitor the progression of the reaction, we identified up to 17 reporter residues showing nonoverlapped monomer and dimer resonances in the ^{1}H–^{15}N HSQC spectrum (Fig. 1 *C*; Fig. S1). Peak volumes over time report on the reaction chemical potential. The equilibrium populations in the reference buffer were estimated from the extrapolation of μ at very long times ($\lim_{t\to\infty}\mu(t) = \Delta G = 0.39$ kcal $\cdot$ mol^{-1}) (32). Yet, a very similar free energy value is obtained after 35 h of reaction time (ΔG = 0.38 kcal mol^{-1}). The obtained fraction of the monomer population, $p_M = 0.68 \pm 0.06$, is largely consistent with the value obtained from SEC data.

As previously shown (32), the peak volumes of NMR resonances over time can be fitted to a good approximation to a biexponential curve to extract the pure kinetic association (k_{asc}) or dissociation (k_{dis}) rates (see Materials and methods and Supporting materials and methods):

$$M + M \underset{k_{dis}^{(eq)\to M}}{\overset{k_{asc}^{M\to(eq)}}{\rightleftharpoons}} [M + D]_{(eq)} \underset{k_{dis}^{D\to(eq)}}{\overset{k_{asc}^{(eq)\to D}}{\rightleftharpoons}} D. \quad (8)$$

To evaluate the association and dissociation rates, we investigated two different reactions starting from either the dimeric (D) or the monomeric (M) species. This simplified model adequately reproduces our experimental data sets (*solid lines* in Fig. 2 *B*), allowing us to extract the reaction rates with high accuracy. As expected, the two opposite initial conditions reported very similar values on the phenomenological kinetic rates (i.e., $k_{dis}^{(eq)\to M} \cong k_{dis}^{D\to(eq)}$ and $k_{asc}^{(eq)\to D} \cong k_{asc}^{M\to(eq)}$) and also the equivalent time evolution of the chemical potential, thus leading to virtually identical estimations of the equilibrium thermodynamics. It is important to note that the equilibrium referred to hereafter corresponds to the apparent state of the system in a time window of ~35 h (biological timescale), which, in this case, does not differ from the extrapolation at $t \to \infty$. We define these kinetic parameters as the reference conditions for the reaction's free energy ($\Delta G^0_{M/D-(eq)} = \Delta G^0_{M-(eq)} = \Delta G^0_{D-(eq)}$) and kinetic rates

$$k^0_{asc} = k^{(eq)\to D}_{asc} = k^{M\to(eq)}_{asc}$$

and

$$k^0_{dis} = k^{(eq)\to M}_{dis} = k^{D\to(eq)}_{dis}.$$

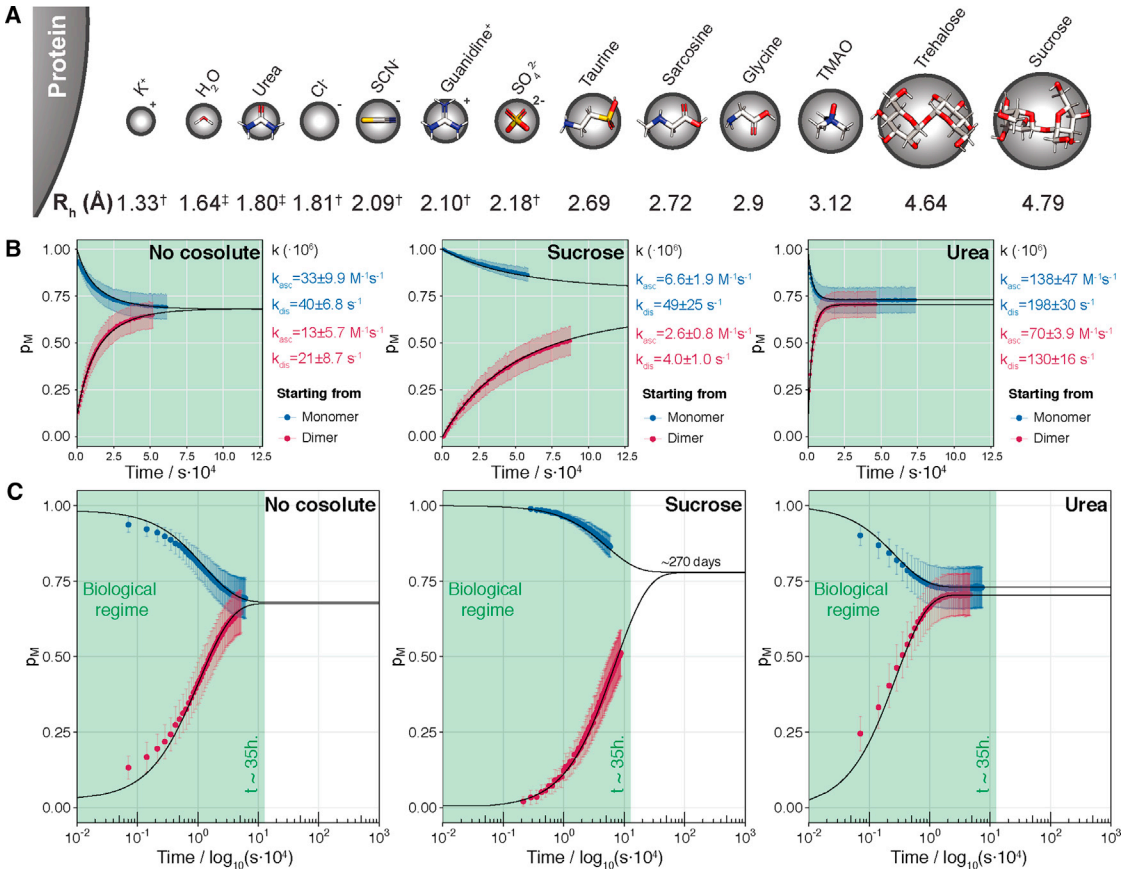

FIGURE 2 Kinetics and thermodynamics of $ProtL_{G55A}$ equilibrium in presence of small molecule cosolutes. (*A*) Schematic representation of the cosolutes used in this study. The size of the cosolute spheres is proportional to the hydrodynamic radius (R_h) calculated from diffusion-ordered NMR spectroscopy (Fig. S5) in 20 mM phosphate buffer (pH 6.0) and 298 K (reference conditions). For ions, the thermochemical radii reported in the literature was used, indicated with a dagger (†) (40,53). The R_h of water and urea are reported to be 1.64 Å (42) and 1.80 Å (54), respectively, and are indicated with a double dagger (‡). (*B*) Monomer populations (p_M) for the reaction starting from the monomer (M ↔ (eq), *blue*) and the reaction starting from the dimer (D ↔ (eq), *red*) in the absence (*first panel*) or presence of different cosolute types. On the right side of each plot, the fitted kinetic rates for both reactions are given (*black line*). (*C*) The same monomer populations plotted against time in logarithmic scale. Note how the thermodynamic equilibrium is always reached. However, the presence of certain cosolutes such as sucrose slows down the reaction up to a biologically irrelevant time of ~270 days. Errors bars indicate the standard deviation (SD) of the different residues used as reporters.

Domain swapping in the presence of cosolutes

The kinetics of the two reactions (M ⇔ (eq) or D ⇔ (eq)) were also monitored in the presence of several cosolutes at 0.5 M concentration (hydrodynamic radius range: 1.33–4.79 Å), with a volume occupancy corresponding to the dilute regime. The protein is completely folded at the tested concentration of cosolutes (including denaturants), indicating that the effects in protein stability are negligible. A rationalized set of small, relatively inert, and highly soluble organic molecules was selected (Fig. 2 *A*; Table S1), including sugar alcohols (sucrose and trehalose), historically used for testing thermodynamic nonideality in protein dimerization (55); amino acids such as glycine, its methylamine sarcosine, and the amino sulfonic acid taurine, which are produced as buffering system of cytoplasm homeostasis under stress conditions (56); and trimethylamine N-oxide (TMAO), which has shown protective properties against denaturing agents such as urea and guanidinium chloride (GuHCl) (57,58) and inorganic ions (K^+, Cl^-, SCN^-, SO_4^{2-}), which also contribute to protein stability (59,60) and oligomerization by the Hofmeister effect (61).

The effect of each crowder on the thermodynamic stability and dimerization kinetics of $ProtL_{G55A}$ was monitored by real-time NMR experiments (Fig. 2 *B*; Table S2), using the strategy described above. For a given crowder and reaction (either *M* ⇔ (*eq*) or *D* ⇔ (*eq*)), the observed kinetics were very similar for the pool of 17 probe residues studied (Fig. 2, *B* and *C*, *error bars*), reinforcing the idea that cosolute effects are largely dominated by the protein backbone and thus mainly affect the global thermodynamics of the protein (62).

The presence of crowders significantly altered the kinetics and the final apparent equilibrium populations of the monomer and dimer species (apparent populations after 35 h), depending not only on the nature of the cosolute but mainly on the initial reaction conditions (Fig. 2, *B* and *C*).

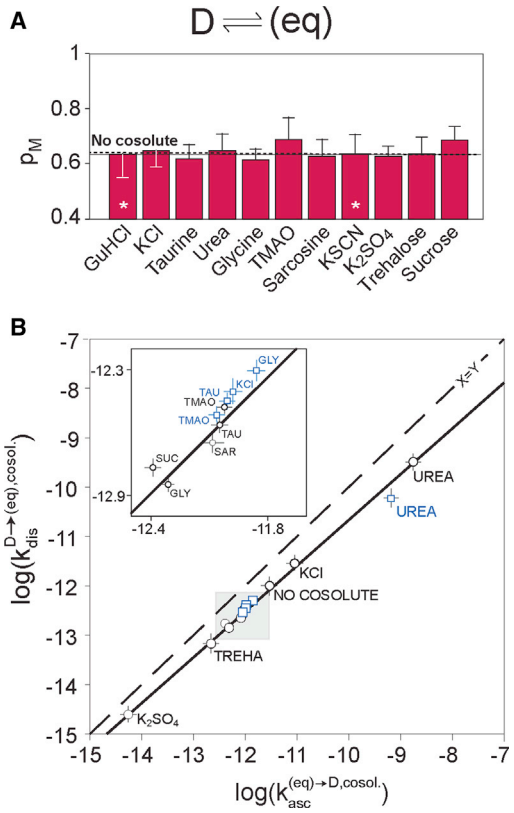

FIGURE 3 Reaction starting from the dimer is under thermodynamic control. (*A*) Average monomer population for the reaction starting from the dimer species, for the apparent equilibria. Dashed line indicates the reference conditions (absence of cosolutes). White asterisks indicate the data sets in which the p_M was directly calculated from peak volumes at the final spectra. The experiments were recorded for at least 12 h (Table S1). (*B*) Onward ($k_{dis}^{D\rightarrow(eq),cosol.}$) and backward ($k_{asc}^{(eq)\rightarrow D,cosol.}$) kinetic rates in the absence ("no cosolute") and presence of 0.5 M cosolutes for the dimer reaction. Blue squares indicate the presence of 0.25 M concentration for a representative subset of cosolutes. Dashed diagonal line indicated the theoretical value for a 1:1 equilibrium. Error bars indicate SDs.

This result is somehow counterintuitive, and it requires further consideration in view of the tested system and current models, so we will further describe the reactions from the two initial conditions separately.

Reaction starting from the dimer ($D \leftrightarrow (eq)$) reaches a cosolute independent equilibrium

A reaction starting from the dimer showed no significant cosolute effects on the chemical potential at the apparent equilibrium as compared to the reference situation (Fig. 2 *B*). In fact, the equilibrium monomer and dimer populations, p_M and p_D, are within error of those determined under reference conditions (Fig. 3 *A*) and already equivalent to the thermodynamic extrapolation to $t \rightarrow \infty$. This is consistent with the minimal changes in excluded volume (ΔV) and ΔASA calculated between two monomers and the domain-swapped dimer (Table S3).

In contrast, cosolutes significantly altered both the association and dissociation rate constants ($k_{asc}^{(eq)\rightarrow D,cosol.}$ and $k_{dis}^{D\rightarrow(eq),cosol.}$) (Fig. 2 *B*), with urea and sulfate producing the fastest and slowest kinetic rates measurable (Fig. 3 *B*). The kinetics of GuHCl and KSCN could not be determined because the equilibrium was already reached at the very initial measured points. The ratio of the two rate constants remains fixed to the same value as in the absence of a crowder (Fig. 3 *B*), and the slope of the corresponding correlation yields a $\Delta G_{D-(eq)}$ value of 0.38 kcal • mol^{-1}, virtually identical to the value determined from the equilibrium populations in the absence of crowders (0.39 kcal • mol^{-1}). This is to be expected because $\Delta G_{D-(eq)} \propto k_{dis}^{D\rightarrow(eq),cosol.}/k_{asc}^{(eq)\rightarrow D,cosol.}$. Changing the cosolute concentration altered the kinetic rates (Fig. 3 *B*) but still has negligible effects on the equilibrium populations.

Our findings support the notion that this reaction is under thermodynamic control, and according to the existing thermodynamic crowding framework (11,23,63), in the presence of a cosolute, the free energy change for the $D \Leftrightarrow (eq)$ reaction in a nonideal (crowded) solution ($\Delta G_{D-(eq)}$) is

$$\Delta G_{D-(eq)} = \Delta G^0_{M/D-(eq)} - RTln\left(\gamma_D / \gamma_M{}^2\right), \qquad (9)$$

where γ_M and γ_D are the activity coefficients of the monomer and the dimer, respectively. As shown in Fig. 2 *B*, experimental data are consistent with $\gamma_D \cong \gamma_M^2$, and, considering the minimal changes in solvent-accessible area and excluded volume between the species under consideration, we hypothesize that the activity coefficients are close to unity: $\gamma_M \cong \gamma_D \cong 1$.

The kinetic rates of dissociation and association, in turn, obey the equations

$$k_{dis}^{D\rightarrow(eq),cosol.} = k_{dis}^0 \times \gamma_D/\gamma_{TS} \text{ and } k_{asc}^{(eq)\rightarrow D,cosol.} = k_{asc}^0 \times \gamma_M^2/\gamma_{TS}, \qquad (10)$$

where γ_{TS} is the activity coefficient of the transition state, which, by definition, depends on the nature and the concentration of the cosolute. According to Eq. 10 and still under the assumption that $\gamma_M \cong \gamma_D \cong 1$, the strong dependence of the kinetic rates with the crowder concentration shall fundamentally arise from γ_{TS}, suggesting that the structure of the transition state may differ significantly from those of the folded species. Table 1 reports the estimated γ_{TS}-values for the cosolute set derived from Eq. 10, providing virtually the same values when calculated from the association and dissociation rates. Urea and high concentrations of KCl show a value of $\gamma_{TS} < 1$, which we interpret in terms of favorable interactions between the cosolutes and the largely unfolded transition state that ultimately result in an acceleration of the reaction rate. In contrast, sugars, amino acids, and stabilizing ions exhibit values of $\gamma_{TS} > 1$, thus producing a reduction of the kinetic rate. Given that the dominant

TABLE 1 Activity coefficients of the transition state γ_{TS}

Cosolute	γ_{TS} (0.5 M)	γ_{TS} (0.25 M)
GuHCl	n.a.	n.a.
KCl	0.6 ± 0.03	1.0 ± 0.02
Taurine	1.7 ± 0.03	1.6 ± 0.01
Urea	0.1 ± 0.07	0.1 ± 0.06
Glycine	2.3 ± 0.05	1.4 ± 0.03
TMAO	1.6 ± 0.04	1.7 ± 0.08
Sarcosine	1.8 ± 0.02	n.a.
KSCN	n.a.	n.a.
K_2SO_4	20.5 ± 0.14	n.a.
Trehalose	3.2 ± 0.06	n.a.
Sucrose	2.3 ± 0.04	n.a.

Error bars indicate SDs. n.a., not applicable.

mechanism for these crowders (64) is excluded volume (65) (even though other mechanisms likely also play a role), these values suggest a contributing excluded volume term from the transition state, whose structure may be significantly bulkier than that of the folded species.

We have further investigated the transition state attempting to obtain a structural model of it by computing the dimer dissociation reaction using GaMD. After a transitory period of around 25 μs in which some of the interactions between the interlaced β-sheets vanish, the trajectory becomes stable for more than 75 ms (Fig. S2, *A–C*). The obtained structural model (Fig. S2 *D*) is an extended dimer stabilized by intermolecular interactions involving T48, K61, and F62 allocated in the remaining interlaced β-sheets. Consistently, when monitored the reaction for $ProtL_{G55A/K61A}$, the monomer population raised up to $p_M = 0.71$ (Fig. S3), suggesting weaker interactions in the dimer interface for the double mutant. This structure exposes 26% more area to the solvent than the fully formed dimer, thus providing a mechanistic rationale to explain the rate dependence with the crowders. Yet, we expected this value to be higher, in line with the idea that near-complete monomer unfolding is required for domain swapping (25). Consistent with this, the large free energy barrier for the transition state ($\Delta G^{\neq} \cong 25$ kcal mol^{-1}), as determined by temperature dependence of the reaction rates (Fig. S4), suggests that the conformation obtained by molecular dynamics simulations might not reflect the rate-limiting step of the reaction, which would be determined by the partial unfolding of the monomer. These data suggest the existence of an intermediate state with partial unfolding before (or after) a largely unfolded transition state. Irrespective of the exact value of surface exposed, this structural model supports our hypothesis that cosolute effects on kinetic rates arise because of a more expanded transition state, and, in consequence, it is more sensitive to crowder-induced excluded volume effects.

Reaction starting from the monomer (*D* ↔ (*eq*)) is kinetically trapped in the biological timescale

When the dimerization equilibrium of $ProtL_{G55A}$ starts from purified monomer, both the kinetic rates and the final equilibrium populations are dependent on the nature and on the concentration of the added cosolute (Fig. 2, *B* and *C*). We claim that these initial conditions produce a reaction that is kinetically trapped (diffusion limited) because the association reaction is bimolecular and the experimental data are consistent with the reaction being limited by the encounter between the two between two partially unfolded intermediates of $ProtL_{G55A}$. Actually, at longer times (i.e., $t \rightarrow \infty$), the thermodynamic equilibrium populations can be extrapolated (Figs. 2 *C* and 4 *A*), but these times become meaningless in the biological timescale (i.e., >100 days).

The encounter rate typically shows an exponential dependence with the concentration of crowder (23)

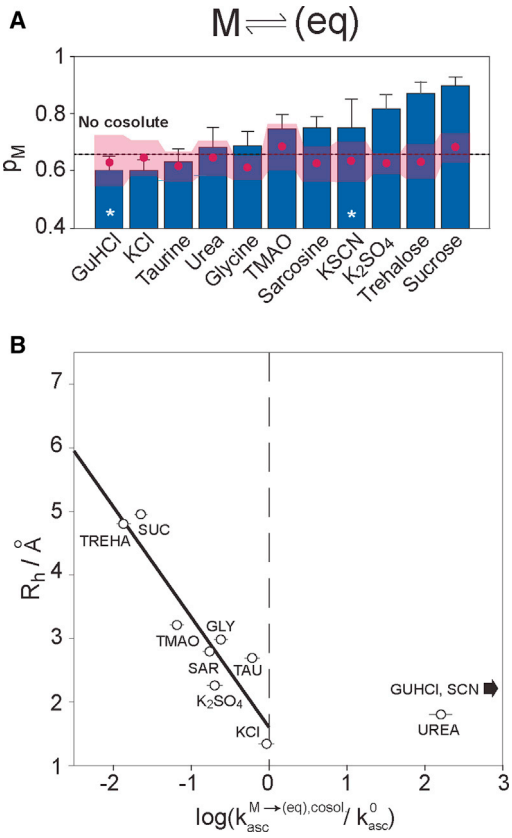

FIGURE 4 Reaction starting from the monomer is under kinetic control. (*A*) Average equilibrium monomer population for the reaction starting from the monomer (*bars*). The reference dimer reaction values and deviations are indicated with points and shades, respectively. Dashed line indicates the reference conditions (absence of cosolutes). White asterisks indicate the data sets in which the p_M was directly calculated from peak volumes at the final spectra. The experiments were recorded for at least 12 h (Table S1). (*B*) Onward ($k_{asc}^{M\rightarrow(eq),cosol.}$) kinetic rates normalized by the standard condition value as function of the hydrodynamic radius of the cosolutes. For salts, the weighted average of the thermochemical radii of participating ions was taken into account. The association rate is inversely proportional to the occupied volume of the cosolute, suggesting diffusion-mediated effects. However, denaturants such as urea, guanidine, and thiocyanate accelerate the association rate by partial unfolding of activated monomers (i.e., more efficient monomer encounters). Error bars indicate SDs.

$$k_{asc}^{M\rightarrow(eq),cosol.} \cong k_{asc}^{0} \times e^{-g[cosol.]}, \quad (11)$$

where g is the proportionality factor to account for the encounter rate (of the intermediate species, vide infra) in the presence of the cosolute. Even though the encounter rate is a purely kinetic constant, it will also determine the apparent final populations that become kinetically accessible. Such modulation is very accentuated, and at 0.5 M of cosolute, a moderate crowder concentration, the p_M deviates from the 0.65 found at reference conditions (i.e., no cosolutes) up to 0.9 ± 0.05 (sucrose) or down to 0.6 ± 0.08 (GuHCl) (Fig. 4 *A*).

The g factor is a function of the relative sizes and shapes of the protein and the cosolutes (23). We have used diffusion-ordered spectroscopy (66) to determine the translational diffusion coefficients for the different cosolutes under consideration that were used to estimate the hydrodynamic ratios (R_h) (Fig. 2 *A*; Table S4; Fig. S5). Because of fast signal exchange or the absence of an NMR observable, the R_h-values for the ions and the guanidine and urea were taken from the literature (40,53,54). The extent to which a given cosolute affects the association rate (here measured as the difference between both rates in logarithm scale, $log(k_{asc}^{M\rightarrow(eq),cosol.}/k_{asc}^{0})$) shows a good linear correlation with the R_h for most of the cosolutes (Fig. 4 *B*). This is consistent with our hypothesis that the encounter complex formation is the limiting factor of the $M \Leftrightarrow (eq)$ reaction. The presence of these cosolutes in the medium oppose the formation of the encounter complex, thus decelerating the association rate. In contrast, the denaturing agents (GuHCl, SCN, and urea) do not abide this correlation and even increase $k_{asc}^{M\rightarrow(eq),cosol.}$. We thus argue that, even though the passive diffusion described above also occurs for these cosolutes, the dominant mechanism for denaturants is the preferential binding to the protein, which unfolds and accelerates the path to the transition state.

Data from the dimer and monomer reaction emphasize 1) the kinetic rates are modulated by the encounter of partially unfolded monomer intermediates, 2) a largely unfolded transition state exists, and 3) diffusion and partial denaturation counterbalance the effect of small cosolutes in domain-swapping oligomerization.

Thus, a mechanistic model considering the existence of intermediates would explain the kinetic rates more realistically.

$$\mathrm{M} + \mathrm{M} \underset{k^{I\rightarrow M}}{\overset{k^{M\rightarrow I}}{\rightleftarrows}} \mathrm{I} + \mathrm{I} \underset{k^{D\rightarrow I}}{\overset{k^{I\rightarrow D}}{\rightleftarrows}} \mathrm{D}. \quad (12)$$

The intermediate is partially unfolded and, therefore, it will expose more area to the solvent. Urea, by preferential interaction with the intermediate as compared to the monomer, accelerates the rate toward equilibrium (i.e., increases $k^{M\rightarrow I}/k^{I\rightarrow M}$ and $k^{D\rightarrow I}/k^{I\rightarrow D}$) and accelerates attainment of equilibrium (see Supporting materials and methods). Sucrose has the opposite effect, retarding the attainment of equilibrium (i.e., it kinetically modulates the reaction by diffusion and preferentially destabilizes the intermediate as compared to the monomer because of excluded volume). The effect of the rest of the cosolutes on the apparent equilibrium reached in the homeostatic timescale will depend on their capacity to preferentially stabilize or denature the intermediate and on their modulation of the diffusion, the latter imposed by their hydrodynamic size.

It is also educational to compare sulfate and TMAO. Sulfate is a kosmotropic ion in the Hoffmeister series, and TMAO is a known protein stabilizer. By excluded volume, both of them will depopulate the intermediate, and this destabilization, combined with the abovementioned diffusion effects, will retard the attainment of equilibrium. TMAO has a larger R_h, and a major kinetic bottleneck capacity is observed (Fig. 4 *B*). Unfortunately, the observation of such intermediates is impaired by their low populations, i.e., the exact kinetic rates (i.e., $k^{M\rightarrow I}$, $k^{I\rightarrow M}$, $k^{I\rightarrow D}$, and $k^{D\rightarrow I}$) cannot be easily determined. Several approaches to quantify low-populated states are available and might be of interest for future studies (67).

CONCLUSIONS

We have investigated the effect of a large set of cosolutes, always smaller in size with respect to the protein, on the thermodynamics and kinetics of a protein homo-oligomerization reaction. The main finding is that the initial conditions modulate the kinetic rates and ultimately determine the populations of the reaction species at the apparent equilibrium reached in a biological timescale (Fig. 3 *A* vs. Fig. 4 *A*). Our results agree well with the seminal existing work (20,68) and are applicable to a large number of cosolutes, including osmolytes, Hofmeister salts, and denaturing agents.

An aggregation process must start with an excess of the monomeric species (Fig. 5 *A*). According to our model, at this stage and in a crowded environment, the encounter complex between the intermediate species will become the limiting factor and the reaction will have maximal sensitivity to the composition (and concentration) of the cytosol, which will determine the nonequilibrium population of the oligomer (Fig. 5, *B* and *C*). Many of the cytosolic cosolutes act through passive diffusion, impeding the formation of an effective encounter complex and thus providing a rationale for the slow triggering kinetics found in many intracellular aggregation processes (Fig. 5 *B*). Yet, the cytosol is very dynamic, with constant modulation of the protein expression over time and the possibility of accumulating some of the species locally, either via compartmentalization or by formation of protein gradients. Those could ultimately tune up the dependence of the oligomerization reaction to the cosolute with local resolution.

Our results also highlight the importance of both the geometry of the transition state and the existence of low-populated partially unfolded intermediates to understand the

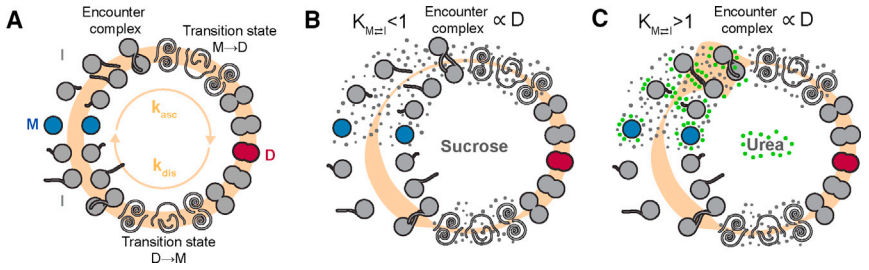

FIGURE 5 Model for the dimerization equilibrium via domain swapping of $ProtL_{G55A}$. (*A*) Schematic representation of the monomer-dimer interconversion equilibrium. In the clockwise direction, two monomers undergo partial unfolding to generate a low-populated intermediate that will efficiently encounter to generate a substantial unfolded transition state. Similarly, the dimer undergoes the opposite symmetrical path in the absence of cosolutes. Orange line width indicate the phenomenological kinetic rates (k_{asc} and k_{dis}) contribution. (*B* and *C*) Schematic representation of the equilibrium in presence of an "inert" cosolute (sucrose) or denaturing agent (urea). Small gray circles emphasize the steps at which the cosolute has substantial contributions in equilibrium kinetics. Green circles represent preferential interactions of urea in the partial unfolding process of the monomer, generating efficient encounters of monomer units.

cosolute effects on domain-swapping reactions, as previously theoretically stated (69,70). This is of particular importance for aggregation processes of folded proteins, in which the initial and the final states may maintain unaltered the relevant geometrical parameters that define the relationship with the crowder agents (i.e., solvent-accessible area and protein volume), yet the reaction rates and eventually the accessible populations are highly sensitive to the cosolute composition. Once more, our experimental results agree with the theoretical framework and point toward a largely unfolded transition state, which is consistent with other protein systems that undergo domain swapping via protein unfolding (28). In turn, the determined activity coefficients of the transition state can be interpreted in terms of the relative solvation of the transition state as compared to the reactants in the crowded environment, a key factor in the cosolute modulation of the reaction rates.

Impaired proteostasis is often the cause of diseases associated with excessive protein misfolding and degradation leading to loss-of-function phenotypes, as well as aggregation-associated degenerative disorders (4). It is often the case that these aggregates are composed of folded proteins, for which changes in the geometrical parameters between the aggregate and the monomers are small (71). We believe that the conclusions drawn from our study using $ProtL_{G55A}$ as a model system may be applicable to these relevant biological processes.

Finally, it is also important to remark on the generality of the result, as it can be applied to cosolutes of very varied nature. Despite their intrinsic differences and the inherent mechanistic complexity that most of these cosolutes have, their effect on oligomerization reaction kinetics and thermodynamics can be largely understood by invoking nonspecific mechanisms such as excluded volume, preferential interactions, and preferential exclusion, which can explain the specific effect of a cosolute in terms of purely geometrical factors. Interestingly, this model is also valid for denaturant agents (Fig. 5 *C*), consistent with the results obtained after more than 50 years of research (72). Here, we complement this well-stablished model by underlining the importance that the initial oligomeric state has in the denaturant effect on these processes.

SUPPORTING MATERIAL

Supporting material can be found online at https://doi.org/10.1016/j.bpj.2021.03.020.

AUTHOR CONTRIBUTIONS

B.M., V.D., and N.Z prepared the samples. Data were collected by B.M., G.B.-S., V.D., and N.Z, with O.M. assisting. B.M. and G.B.-S. analyzed the real-time NMR data. O.M. designed the samples. F.P. and G.J.-O. run the molecular dynamics simulations. B.M, G.B.-S, G.O., M.T., and O.M. discussed the results. O.M. coordinated the research. B.M. and O.M. wrote the manuscript with contributions from all authors.

ACKNOWLEDGMENTS

Support was provided by the Department of Industry, Tourism and Trade of the Government of the Autonomous Community of the Basque Country (Elkartek BG2019) and the Severo Ochoa Excellence Accreditation from MCIU (SEV-2016-0644). O.M. acknowledges the Agencia Estatal de Investigación for grants CTQ2015-68756-R and RTI2018-101269-B-I00, and B.M acknowledges the Austrian Science Fund grant W1258, "DK: Integrative Structural Biology." R.K. gratefully acknowledges the Austrian Federal Ministry of Science, Research and Economy and the National Foundation for Research, Technology and Development. M.T. acknowledges support by the Austrian Research Promotion Agency FFG (project 858017, West-Austrian BioNMR). G.J.-O. acknowledges the Agencia Estatal de Investigación for grant RTI2018-099592-B-C22 and Mizutani Foundation for Glycoscience for grant 20007.

REFERENCES

1. Balchin, D., M. Hayer-Hartl, and F. U. Hartl. 2016. In vivo aspects of protein folding and quality control. *Science.* 353:aac4354.
2. Yancey, P. H. 2005. Organic osmolytes as compatible, metabolic and counteracting cytoprotectants in high osmolarity and other stresses. *J. Exp. Biol.* 208:2819–2830.
3. Ellis, R. J., and A. P. Minton. 2006. Protein aggregation in crowded environments. *Biol. Chem.* 387:485–497.
4. Dobson, C. M. 2003. Protein folding and misfolding. *Nature.* 426:884–890.
5. Breydo, L., K. D. Reddy, …, V. N. Uversky. 2014. The crowd you're in with: effects of different types of crowding agents on protein aggregation. *Biochim. Biophys. Acta.* 1844:346–357.
6. Wang, W., S. Nema, and D. Teagarden. 2010. Protein aggregation–pathways and influencing factors. *Int. J. Pharm.* 390:89–99.

7. Ellis, R. J. 2001. Macromolecular crowding: obvious but underappreciated. *Trends Biochem. Sci.* 26:597–604.
8. Minton, A. P. 2013. Quantitative assessment of the relative contributions of steric repulsion and chemical interactions to macromolecular crowding. *Biopolymers.* 99:239–244.
9. Schellman, J. A. 2003. Protein stability in mixed solvents: a balance of contact interaction and excluded volume. *Biophys. J.* 85:108–125.
10. Record, M. T., Jr., C. F. Anderson, and T. M. Lohman. 1978. Thermodynamic analysis of ion effects on the binding and conformational equilibria of proteins and nucleic acids: the roles of ion association or release, screening, and ion effects on water activity. *Q. Rev. Biophys.* 11:103–178.
11. Schreiber, G. 2002. Kinetic studies of protein-protein interactions. *Curr. Opin. Struct. Biol.* 12:41–47.
12. Phillip, Y., E. Sherman, …, G. Schreiber. 2009. Common crowding agents have only a small effect on protein-protein interactions. *Biophys. J.* 97:875–885.
13. Zhao, Q., R. Fujimiya, …, N. Nishida. 2020. Real-time in-cell NMR reveals the intracellular modulation of GTP-bound levels of RAS. *Cell Rep.* 32:108074.
14. Yang, Y., S.-N. Chen, …, D. Goldfarb. 2020. In-cell destabilization of a homodimeric protein complex detected by DEER spectroscopy. *Proc. Natl. Acad. Sci. USA.* 117:20566–20575.
15. Rivas, G., and A. P. Minton. 2016. Macromolecular crowding in vitro, in vivo, and in between. *Trends Biochem. Sci.* 41:970–981.
16. Zhou, H.-X., G. Rivas, and A. P. Minton. 2008. Macromolecular crowding and confinement: biochemical, biophysical, and potential physiological consequences. *Annu. Rev. Biophys.* 37:375–397.
17. Miklos, A. C., M. Sarkar, …, G. J. Pielak. 2011. Protein crowding tunes protein stability. *J. Am. Chem. Soc.* 133:7116–7120.
18. Arakawa, T., and S. N. Timasheff. 1985. Mechanism of poly(ethylene glycol) interaction with proteins. *Biochemistry.* 24:6756–6762.
19. Rydeen, A. E., E. M. Brustad, and G. J. Pielak. 2018. Osmolytes and protein-protein interactions. *J. Am. Chem. Soc.* 140:7441–7444.
20. Minton, A. P. 1983. The effect of volume occupancy upon the thermodynamic activity of proteins: some biochemical consequences. *Mol. Cell. Biochem.* 55:119–140.
21. Elcock, A. H. 2010. Models of macromolecular crowding effects and the need for quantitative comparisons with experiment. *Curr. Opin. Struct. Biol.* 20:196–206.
22. Phillip, Y., and G. Schreiber. 2013. Formation of protein complexes in crowded environments–from in vitro to in vivo. *FEBS Lett.* 587:1046–1052.
23. Minton, A. P. 1998. Molecular crowding: analysis of effects of high concentrations of inert cosolutes on biochemical equilibria and rates in terms of volume exclusion. *Methods Enzymol.* 295:127–149.
24. Hoffman, L., X. Wang, …, M. N. Waxham. 2015. Relative cosolute size influences the kinetics of protein-protein interactions. *Biophys. J.* 109:510–520.
25. Liu, L., I.-J. L. Byeon, …, A. M. Gronenborn. 2012. Domain swapping proceeds via complete unfolding: a 19F- and 1H-NMR study of the Cyanovirin-N protein. *J. Am. Chem. Soc.* 134:4229–4235.
26. Liu, Y., and D. Eisenberg. 2002. 3D domain swapping: as domains continue to swap. *Protein Sci.* 11:1285–1299.
27. Sinha, N., C. J. Tsai, and R. Nussinov. 2001. A proposed structural model for amyloid fibril elongation: domain swapping forms an interdigitating β-structure polymer. *Protein Eng.* 14:93–103.
28. Campos, L. A., R. Sharma, …, V. Muñoz. 2019. Engineering protein assemblies with allosteric control via monomer fold-switching. *Nat. Commun.* 10:5703.
29. Berg, O. G. 1990. The influence of macromolecular crowding on thermodynamic activity: solubility and dimerization constants for spherical and dumbbell-shaped molecules in a hard-sphere mixture. *Biopolymers.* 30:1027–1037.
30. Guseman, A. J., G. M. Perez Goncalves, …, G. J. Pielak. 2018. Protein shape modulates crowding effects. *Proc. Natl. Acad. Sci. USA.* 115:10965–10970.
31. Guseman, A. J., and G. J. Pielak. 2017. Cosolute and crowding effects on a side-by-side protein dimer. *Biochemistry.* 56:971–976.
32. Moschen, T., and M. Tollinger. 2014. A kinetic study of domain swapping of Protein L. *Phys. Chem. Chem. Phys.* 16:6383–6390.
33. O'Neill, J. W., D. E. Kim, …, K. Y. J. Zhang. 2001. Single-site mutations induce 3D domain swapping in the B1 domain of protein L from Peptostreptococcus magnus. *Structure.* 9:1017–1027.
34. Palmer, A. G., III 2014. Chemical exchange in biomacromolecules: past, present, and future. *J. Magn. Reson.* 241:3–17.
35. Toyama, B. H., and M. W. Hetzer. 2013. Protein homeostasis: live long, won't prosper. *Nat. Rev. Mol. Cell Biol.* 14:55–61.
36. Delaglio, F., S. Grzesiek, …, A. Bax. 1995. NMRPipe: a multidimensional spectral processing system based on UNIX pipes. *J. Biomol. NMR.* 6:277–293.
37. Vranken, W. F., W. Boucher, …, E. D. Laue. 2005. The CCPN data model for NMR spectroscopy: development of a software pipeline. *Proteins.* 59:687–696.
38. Hardy, R. C., and R. L. Cottington. 1949. Viscosity of deuterium oxide and water in the range 5 to 125 C. *J. Res. Natl. Bur. Stand.* 42:573–578.
39. Wang, C. K., S. E. Northfield, …, D. J. Craik. 2014. Translational diffusion of cyclic peptides measured using pulsed-field gradient NMR. *J. Phys. Chem. B.* 118:11129–11136.
40. Roobottom, H. K., H. D. B. Jenkins, …, L. Glasser. 1999. Thermochemical radii of complex ions. *J. Chem. Educ.* 76:1570.
41. Creamer, T. P., R. Srinivasan, and G. D. Rose. 1997. Modeling unfolded states of proteins and peptides. II. Backbone solvent accessibility. *Biochemistry.* 36:2832–2835.
42. Price, W. S., H. Ide, and Y. Arata. 2000. Translational and rotational motion of isolated water molecules in nitromethane studied using 17O NMR. *J. Chem. Phys.* 113:3686–3689.
43. Chen, C. R., and G. I. Makhatadze. 2015. ProteinVolume: calculating molecular van der Waals and void volumes in proteins. *BMC Bioinformatics.* 16:101.
44. Lee, T. S., D. S. Cerutti, …, D. M. York. 2018. GPU-accelerated molecular dynamics and free energy methods in amber18: performance enhancements and new features. *J. Chem. Inf. Model.* 58:2043–2050.
45. Maier, J. A., C. Martinez, …, C. Simmerling. 2015. ff14SB: improving the accuracy of protein side chain and backbone parameters from ff99SB. *J. Chem. Theory Comput.* 11:3696–3713.
46. Jorgensen, W. L., J. Chandrasekhar, …, M. L. Klein. 1983. Comparison of simple potential functions for simulating liquid water. *J. Chem. Phys.* 79:926–935.
47. Andersen, H. C. 1980. Molecular dynamics simulations at constant pressure and/or temperature. *J. Chem. Phys.* 72:2384–2393.
48. Andrea, T. A., W. C. Swope, and H. C. Andersen. 1983. The role of long ranged forces in determining the structure and properties of liquid water. *J. Chem. Phys.* 79:4576–4584.
49. Miyamoto, S., and P. A. Kollman. 1992. Settle: an analytical version of the SHAKE and RATTLE algorithm for rigid water models. *J. Comput. Chem.* 13:952–962.
50. Darden, T., D. York, and L. Pedersen. 1993. Particle mesh Ewald: an N·log(N) method for Ewald sums in large systems. *J. Chem. Phys.* 98:10089–10092.
51. Miao, Y., W. Sinko, …, J. A. McCammon. 2014. Improved reweighting of accelerated molecular dynamics simulations for free energy calculation. *J. Chem. Theory Comput.* 10:2677–2689.
52. Miao, Y., V. A. Feher, and J. A. McCammon. 2015. Gaussian accelerated molecular dynamics: unconstrained enhanced sampling and free energy calculation. *J. Chem. Theory Comput.* 11:3584–3595.
53. Marcus, Y. 2012. The guanidinium ion. *J. Chem. Thermodyn.* 48:70–74.

54. Schultz, S. G., and A. K. Solomon. 1961. Determination of the effective hydrodynamic radii of small molecules by viscometry. *J. Gen. Physiol.* 44:1189–1199.

55. Shearwin, K. E., and D. J. Winzor. 1988. Effect of sucrose on the dimerization of α-chymotrypsin. Allowance for thermodynamic nonideality arising from the presence of a small inert solute. *Biophys. Chem.* 31:287–294.

56. Somero, G. N. 1986. Protons, osmolytes, and fitness of internal milieu for protein function. *Am. J. Physiol.* 251:R197–R213.

57. Ma, J., I. M. Pazos, and F. Gai. 2014. Microscopic insights into the protein-stabilizing effect of trimethylamine N-oxide (TMAO). *Proc. Natl. Acad. Sci. USA.* 111:8476–8481.

58. Pincus, D. L., C. Hyeon, and D. Thirumalai. 2008. Effects of trimethylamine N-oxide (TMAO) and crowding agents on the stability of RNA hairpins. *J. Am. Chem. Soc.* 130:7364–7372.

59. Ortega, G., T. Diercks, and O. Millet. 2015. Halophilic protein adaptation results from synergistic residue-ion interactions in the folded and unfolded states. *Chem. Biol.* 22:1597–1607.

60. Tadeo, X., B. López-Méndez, …, O. Millet. 2009. Structural basis for the aminoacid composition of proteins from halophilic archea. *PLoS Biol.* 7:e1000257.

61. Tadeo, X., B. López-Méndez, …, O. Millet. 2009. Protein stabilization and the Hofmeister effect: the role of hydrophobic solvation. *Biophys. J.* 97:2595–2603.

62. Auton, M., and D. W. Bolen. 2005. Predicting the energetics of osmolyte-induced protein folding/unfolding. *Proc. Natl. Acad. Sci. USA.* 102:15065–15068.

63. Jiao, M., H. T. Li, …, Y. Liang. 2010. Attractive protein-polymer interactions markedly alter the effect of macromolecular crowding on protein association equilibria. *Biophys. J.* 99:914–923.

64. Patel, C. N., S. M. Noble, …, G. J. Pielak. 2002. Effects of molecular crowding by saccharides on α-chymotrypsin dimerization. *Protein Sci.* 11:997–1003.

65. Tadeo, X., M. Pons, and O. Millet. 2007. Influence of the Hofmeister anions on protein stability as studied by thermal denaturation and chemical shift perturbation. *Biochemistry.* 46:917–923.

66. Sinnaeve, D. 2012. The Stejskal-Tanner equation generalized for any gradient shape-an overview of most pulse sequences measuring free diffusion. *Concepts Magn. Reson. Part A.* 40A:39–65.

67. Baldwin, A. J., and L. E. Kay. 2009. NMR spectroscopy brings invisible protein states into focus. *Nat. Chem. Biol.* 5:808–814.

68. Schreiber, G., G. Haran, and H. X. Zhou. 2009. Fundamental aspects of protein-protein association kinetics. *Chem. Rev.* 109:839–860.

69. Zimmerman, S. B., and A. P. Minton. 1993. Macromolecular crowding: biochemical, biophysical, and physiological consequences. *Annu. Rev. Biophys. Biomol. Struct.* 22:27–65.

70. Tang, C., J. Iwahara, and G. M. Clore. 2006. Visualization of transient encounter complexes in protein-protein association. *Nature.* 444:383–386.

71. Macias, I., A. Laín, …, O. Millet. 2019. Hereditary tyrosinemia type I-associated mutations in fumarylacetoacetate hydrolase reduce the enzyme stability and increase its aggregation rate. *J. Biol. Chem.* 294:13051–13060.

72. Schellman, J. A. 2002. Fifty years of solvent denaturation. *Biophys. Chem.* 96:91–101.